This article has been accepted for publication in IEEE Transactions on Applied Superconductivity. This is the author's version which has not been fully edited and content may change prior to final publication. Citation information: DOI 10.1109/TASC.2023.3258369

2MPo2C-07

# Impact of Calcium Doping of $YBa_2Cu_3O_{7-\delta}$ Multilayer Thin Films on the Flux Pinning Landscape at 65–5 K, 0–9 T for Various Applications

Mary Ann Sebastian, Charles Ebbing, Di Zhang Jie Jian, Jijie Huang, Yifan Zhang, Haiyan Wang, Victor Ogunjimi, Mohan Panth, Bibek Gautam, Judy Wu, and Timothy Haugan

***Abstract*— An important research goal in the applications of high temperature superconductor $YBa_2Cu_3O_{7-\delta}$ (YBCO) thin films is increasing both the critical current density and also the isotropic nature of the film. YBCO is inherently anisotropic due to its layered perovskite structure. The critical current density of YBCO thin films is enhanced by increasing the flux pinning sites in the film by the addition of insulating nano-phase materials, such as $BaZrO_3$ (BZO) nanorods, which are also anisotropic in nature. Using a multilayer pulsed laser deposition technique has been shown to produce films with inclusions that are more isotropic in nature. However, the defective BZO nanorod interface, resulting from its lattice mismatch with YBCO, prevents obtaining optimum pinning force. This research explores the effect of Ca doped YBCO space layers in the multilayer composite film, on the BZO nanorod/YBCO interface, over a wide range of conditions of 65–5 K and 0– 9T that are suitable for various applications. The interplay of combining these three variables: $BaZrO_3$ addition to YBCO, multilayer film growth resulting from varying pulsed laser deposition conditions, and employing calcium doped YBCO space layers, and the resulting impact on film microstructures and superconducting properties, will be presented.**

***Index Terms*- BZO/YBCO interface, pinning efficiency, strain field, lattice mismatch, vortex pinning**

## INTRODUCTION

Enhancing critical current density ($J_c$) and reducing its anisotropy at various angular orientations of the magnetic field has been an area of tremendous research in high-temperature superconductors (HTS). Both self-field and in-field $J_c$ must be enhanced at different temperatures to meet the requirements for a variety of applications. These requirements include power transmission cables (<1 T, 77 K), large motors (4–5 T, 20–77 K), generators (4–5 T, 20–50 K), fault current limiters (0.1–3 T, 20–77 K) and superconducting magnetic energy storage systems (5–10 T, 20–77 K) [1]–[3]. In order to meet these requirements, the addition of impurity dopants to form so-called artificial pinning centers (APCs) is essential to pin the magnetic vortices at applied magnetic fields at which the naturally occurring growth defects cannot provide strong pins. Various APCs of different morphologies, including c-axis aligned one-dimensional nanorods (1D-APCs), ab-plane aligned two-dimensional planar defects (2D-APCs), and three-dimensional nanoparticles (3D-APCs) have been reported through the addition of impurity dopants such as $BaZrO_3$ (BZO), $BaHfO_3$ (BHO), $BaSnO_3$ (BSO), $YBa_2(Nb/Ta)O_6$, $Y_2O_3$, etc. in REBCO (RE=rare-earth elements: Y, Er, Gd, Nd, Sm) and enhanced pinning has been achieved in these APC/REBCO nanocomposite films [4]–[13]. Among others, BZO-1D APCs have been comprehensively studied after the

This research was supported in part by NSF contract Nos: NSF-DMR-1508494, 1909292 and 2016453, and NSF-ECCS-1809293, by AFRL Aerospace Systems Directorate, and by the Air Force Office of Scientific Research (AFOSR) LRIR #18RQCOR100. (*Corresponding author: Mary Ann Sebastian*)

Mary Ann Sebastian is with the University of Dayton Research Institute Dayton, OH 45469, USA and with the Air Force Research Laboratory, AFRL/RQQM, OH 45433, USA (email: mailto: maryann.sebastian@udri.udayton.edu)
Charles Ebbing is with the University of Dayton Research Institute Dayton, OH 45469, USA (email: Charles.Ebbing@udri.udayton.edu)
Timothy Haugan is with the Air Force Research Laboratory, AFRL/RQQM, OH 45433, USA (email: timothy.haugan@us.af.mil)
Mohan Panth, Victor Ogunjimi, Bibek Gautam and Judy Wu are with the Department of Physics and Astronomy, the University of Kansas, Lawrence, Kansas 66045, USA (email: panthm@ku.edu; victorogunjimi@ku.edu; gautambik@gmail.com; jwu@ku.edu)
Di Zhang, Jie Jian, Jijie Huang, Yifan Zhang and Haiyan Wang are with the School of Materials Engineering, Purdue University, West Lafayette, IN 47907, USA (email: zhan2923@purdue.edu; jian1@purdue.edu; haun1027@purdue.edu; zhan2592@purdue.edu; hwang00@purdue.edu)

© 2023 IEEE. Personal use is permitted, but republication/redistribution requires IEEE permission. See https://www.ieee.org/publications/rights/index.html for more information.
Authorized licensed use limited to: University of Kansas Libraries. Downloaded on March 25,2023 at 14:26:22 UTC from IEEE Xplore. Restrictions apply.

This article has been accepted for publication in IEEE Transactions on Applied Superconductivity. This is the author's version which has not been fully edited and content may change prior to final publication. Citation information: DOI 10.1109/TASC.2023.3258369



first report by MacManus-Driscoll *et al* [5]. BZO-1D APCs can form as c-axis aligned arrays in a broad range of BZO doping concentration, with areal density proportional approximately linearly to the BZO doping. This allows the areal density of the nanorods to be tuned in order to obtain optimal pinning in applications targeted for specific magnetic fields. However, a defective BZO/YBCO interface formed due to the large lattice mismatch ~7.7% between BZO 1D-APCs and YBCO resulted in reduced pinning performance of the BZO 1D-APCs and degradation of superconducting properties of the BZO/YBCO nanocomposites [14]–[16]. The immediate remedy to this problem would be repairing or avoiding the formation of such a defective interface. Recently, we have developed a multilayer (ML) scheme to dynamically enlarge the c-lattice constant of YBCO after or during the BZO 1D-APC formation through Ca doping into the tensile strained BZO/YBCO interface [17]. The Ca doping is done by incorporating a 10 nm thick $Ca_{0.3}Y_{0.7}Ba_2Cu_3O_{7-x}$ (CaY123) spacer layer into the BZO/YBCO nanocomposite film to allow Ca diffusion during the in-situ film growth. The enlarged c-lattice constant up to 1.24 nm leads to reduced BZO/YBCO lattice mismatch from 7.7% to 1.4% that prevents formation of defects at the BZO/YBCO interface. As a result of the highly coherent BZO/YBCO interface, enhanced $J_c$ and pinning force density ($F_p$) values have been obtained at temperatures of 65–77 K in magnetic fields up to 9 T at H//c-axis and other orientations [18]–[21].

It should be noted that the BZO/YBCO nanocomposites can play an important role in various applications at low temperatures much below 77 K. It is therefore important to understand the pinning properties, such as $J_c$ and $F_p$ at low temperatures. However, measuring $J_c$ at low temperatures requires precaution in wiring, which has limited the $J_c$ measurement to temperatures of 65-77K on BZO/YBCO ML samples [17]–[21]. Motivated by this, we investigate the low-temperature $J_c$ and pinning properties of the 6 vol.% BZO/YBCO ML nanocomposite films at 5 K and 65 K using the magnetic approach. The ML films fabricated at various CaY123 layer thicknesses, and at different laser repetition rates were studied to understand the effect of those parameters on the pinning properties of the film. Remarkably, enhanced $J_c$ and $F_p$ have been observed on all ML samples as compared to their single-layer (SL) BZO/YBCO nano-composite counterparts and the undoped reference YBCO film.

## EXPERIMENTAL

Six vol.% BZO doped YBCO nanocomposite films were deposited on *(100)* $SrTiO_3$ (STO) single crystal substrates using pulsed laser deposition (PLD). Substrates with varying dimensions of 3 mm by 3 mm (quantity 3), 5 mm by 5 mm (quantity 2) and 4 mm by 10 mm (quantity 1), and with a thickness of 0.5 mm, were attached to the heater block with colloidal silver (Fig. 1(a)). The KrF laser (wavelength~248 nm, energy~450 mJ) was used to ablate the target material. The target to the heater distance was 5.5 cm. For comparison, 6 vol.% BZO/YBCO SL nanocomposite and undoped reference YBCO films were also made using PLD for extraction of the Ca doping effect. A schematic of YBCO on STO doped with BZO nanorods and a multilayer (ML) YBCO film doped with BZO and with CaY123 layers can be seen in Fig. 1(b)–(c). The ML BZO/YBCO samples would be otherwise the same to their SL counterpart except with two additional Ca-containing spacer layers inserted in each BZO/YBCO nanocomposite film. Specifically, $Ca_{0.3}Y_{0.7}Ba_2Cu_3O_{7-x}$ (CaY 123) was used as the Ca-containing spacers. These ML samples have a multilayer structure with three ~50 nm thick BZO/YBCO layers separated by two CaY123 spacers. The amount of the Ca was controlled by varying the thickness of the CaY123 layer in the range of 5–15 nm, and the Ca diffusion time by the PLD repetition rate in the range of 1–4 Hz. Basically, the thicker the CaY 123 spacer, the more Ca is in the spacer for diffusion into the BZO/YBCO layer, driven across the interface between BZO/YBCO and the CaY123 spacers. In addition, the higher the repetition rate, the shorter the diffusion time. The total thickness of all the samples is ~160–180 nm. The thickness of the samples was measured by etching with 2% nitric acid and measuring the step height using a profilometer. All ML and SL and undoped YBCO samples were deposited at the substrate temperature of ~825 °C in a 300 mTorr oxygen ($O_2$) environment. The deposition parameters are optimized from our previous works [11, 13, 20, 22]. Eight Hz repetition rate was used for PLD growth of the BZO/YBCO in both SL and ML samples. After the deposition, the samples were annealed for about 30 minutes of dwell time at 500 °C in one-atmosphere $O_2$ pressure. The fabrication conditions are listed in Table I below. The crystallinity and microstructure analysis was done by using x-ray diffraction (XRD) and electron microscopy techniques. Specifically, a Bruker D8 Discover XRD system with a Cu tube (1.5418 Å) and a high-resolution setting at 40 kV and 40 mA was used to conduct $\theta$–$2\theta$ scans from 0 °–80 ° and $2\theta$–ω rocking curve scans of the YBCO *(005)* peak. High-resolution scanning and transmission electron microcopy (STEM) images were collected using a Thermo Fisher Scientific Themis-Z transmission electron microscopy (TEM) system with acceleration voltage up to 300 kV. The cross-sectional TEM samples were prepared using a protocol consisting of manual grinding, polishing, dimpling and a final ion-milling step.

$J_c$ was measured as a function of magnetic field (H) utilizing a Quantum Design Vibrational Sample Magnetometer (VSM) system with the magnetic field applied parallel to the c-direction and ramped from zero field to 9.0 T at temperatures 77K, 65K, 50K, 40K, 30K, 20K 10K, and 5K. Only data for 65 K and 5 K are presented in this paper so as to not clutter the graphs. The advantage of the magnetic approach is to avoid patterning the films using photolithography as is done with transport measurements. In addition, it allows $J_c$ measurement at low temperatures at which the very high $I_c$ may require precaution of wiring in transport measurement. The Bean model was employed to estimate the $J_c$ values [23]–[25].

© 2023 IEEE. Personal use is permitted, but republication/redistribution requires IEEE permission. See https://www.ieee.org/publications/rights/index.html for more information.
Authorized licensed use limited to: University of Kansas Libraries. Downloaded on March 25,2023 at 14:26:22 UTC from IEEE Xplore. Restrictions apply.

This article has been accepted for publication in IEEE Transactions on Applied Superconductivity. This is the author's version which has not been fully edited and content may change prior to final publication. Citation information: DOI 10.1109/TASC.2023.3258369



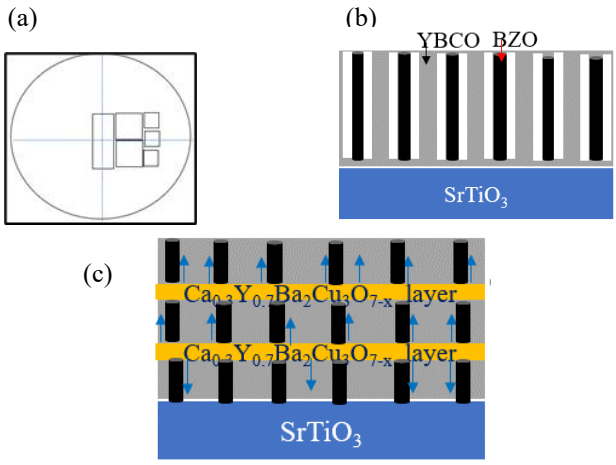


Fig. 1. (a) Arrangement of substrates on the heater block. Schematic of BZO/YBCO SL (b) and ML (c) films. BZO 1D-APCs are shown in black and the CaY123 spaces are in orange [18].

## RESULTS AND DISCUSSION

Table I
SUMMARY OF THE FABRICATED SAMPLE INFO

| BZO/YBCO MLFilm | BZO PLD repetition rate (Hz) | BZO layer thickness (nm) | CaY123 layer thickness (nm) | CaY123 PLD repetition rate (Hz) |
|---|---|---|---|---|
| 6 vol.% BZO + YBCO | 8 | 50 | 10 | 2 |
| 6 vol.% BZO + YBCO | 8 | 50 | 5 | 4 |
| 6 vol.% BZO + YBCO | 8 | 50 | 10 | 4 |
| 6 vol.% BZO + YBCO | 8 | 50 | 15 | 4 |

Fig. 2(a) shows the XRD $\theta$–$2\theta$ spectra of three 6 % BZO/YBCO ML films fabricated at the same laser repetition rate of 4 Hz with varying CaY123 spacer layer thicknesses of 5 nm, 10 nm, and 15 nm by controlling the number of laser pulses via the Neocera laser program based on the pre-calibrated deposition rate (nm/pulse). Fig. 2(b) compares the XRD $\theta$–$2\theta$ spectra of another set of the ML samples all having two CaY123 spacers of 10 nm in thickness while the spacers were made at a different PLD repetition rate of 1 Hz, 2 Hz, and 4 Hz respectively. The XRD $\theta$–$2\theta$ spectra for both sets of the ML samples show *c*-axis oriented epitaxial growth of the films evidenced by the *(00l)* YBCO peaks (#). In addition, the formation of epitaxial BZO 1D-APCs in the YBCO matrix is confirmed by the major BZO peak (*) at $2\theta \sim 46.5^{\circ}$ in all six 6 % ML films. The calculated c-axis lattice constants of the samples made with a laser repetition rate of 4 Hz and CaY123 layers of 5 nm, 10 nm, and 15 nm respectively are 11.762 Å, 11.745 Å, and 11.736 Å respectively. In addition, the calculated *c*-axis lattice constants of the films are 11.734 Å, 11.766 Å and 11.745Å for the three ML samples made with a

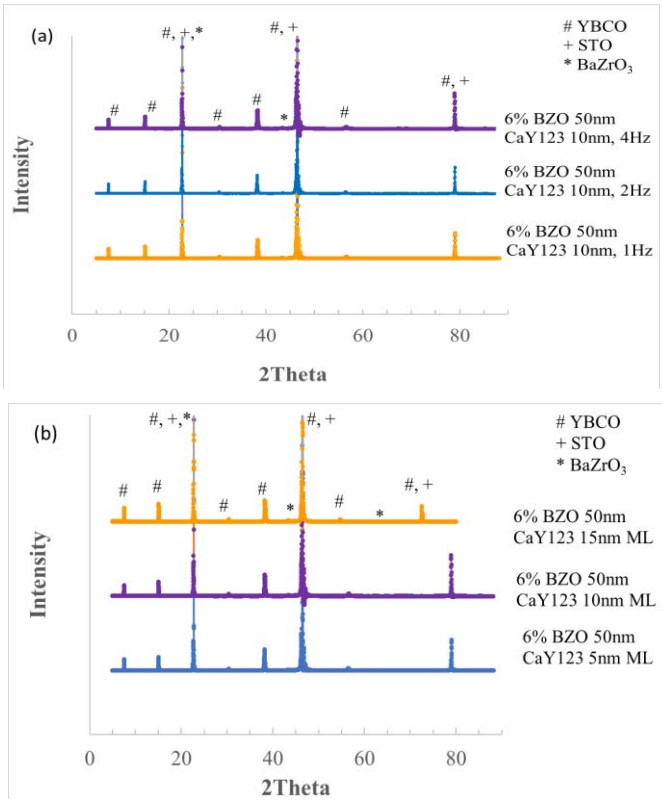


Fig. 2. XRD θ-2θ spectra on 6 vol.% BZO/YBCO ML nanocomposite films of (a) varying CaY 123 spacer layer thicknesses of 5 nm, 10 nm, and 15 nm, (b) varying repetition rates of 1 Hz, 2 Hz, and 4 Hz with 10 nm thick CaY 123 spacer layer thickness.

CaY123 layer of 10 nm and laser repetition rate of 1 Hz, 2 Hz, and 4 Hz respectively.

The crystallinity of the films was further evaluated by calculating the FWHM values of the *(005)* peaks. Specifically, the FWHM value are 0.342 °, 0.379 ° and 0.344 ° for the 6 % ML samples made with a repetition rate of 4 Hz and CaY123 layers of 5 nm, 10 nm, and 15 nm respectively are comparable. Similarly, the FWHM values are 0.261 °, 0.38 ° and 0.379 ° for the 6 % ML samples made with CaY123 layers of 10 nm and repetition rates of 1 Hz, 2 Hz, and 4 Hz respectively. The small values of FWHM in all 6 ML samples suggest that the samples are of the highest crystallinity [26]. The results of XRD characterization of the six ML samples are summarized in Table II and Table III respectively.

Table II
SUMMARY OF STRUCTURAL AND SUPERCONDUCTING PARAMETERS FOR BZO/YBCO SAMPLES WITH 4 HZ OF REPETITION RATE AND CAY123 LAYERS OF 5 NM, 10 NM AND 15 NM IN THICKNESS

| BZO/YBCO ML film | Ca layer thickness (nm) | FWHM | c-lattice (Å) | $T_c$ (K) |
|---|---|---|---|---|
| 6 vol.% BZO + YBCO | 5 | 0.342 | 11.7625 | 86.3 |
| 6 vol.% BZO + YBCO | 10 | 0.379 | 11.7451 | 86.5 |
| 6 vol.% BZO + YBCO | 15 | 0.344 | 11.7369 | 86.2 |

© 2023 IEEE. Personal use is permitted, but republication/redistribution requires IEEE permission. See https://www.ieee.org/publications/rights/index.html for more information.
Authorized licensed use limited to: University of Kansas Libraries. Downloaded on March 25,2023 at 14:26:22 UTC from IEEE Xplore. Restrictions apply.

This article has been accepted for publication in IEEE Transactions on Applied Superconductivity. This is the author's version which has not been fully edited and content may change prior to final publication. Citation information: DOI 10.1109/TASC.2023.3258369



Table III
SUMMARY OF STRUCTURAL AND SUPERCONDUCTING PARAMETERS FOR BZO/YBCO ML SAMPLES WITH 10 NM THICK CAY123 LAYERS MADE USING 1 HZ, 2 HZ, AND 4 HZ PLD REPETITION RATES RESPECTIVELY

| BZO/YBCO ML film | Repetition Rate (Hz) | FWHM | c-lattice (Å) | $T_c$ (K) |
|---|---|---|---|---|
| 6 vol.% BZO + YBCO | 1 | 0.261 | 11.73375 | 87.3 |
| 6 vol.% BZO + YBCO | 2 | 0.380 | 11.7658 | 83.3 |
| 6 vol.% BZO + YBCO | 4 | 0.379 | 11.7451 | 86.5 |

Fig. 3(a)–(c) show the cross-sectional STEM images of a 6 % BZO/YBCO ML film with different magnifications. The film consists of ~ 50 nm thick BZO doped YBCO layers which were deposited at a repetition rate of 8 Hz and ~ 10 nm thick CaY123 spacer layers which were deposited at a repetition rate of 2 Hz. BZO 1D-APCs formed through each of the three BZO/YBCO layers are clearly visible in the ML BZO/YBCO nanocomposite film.

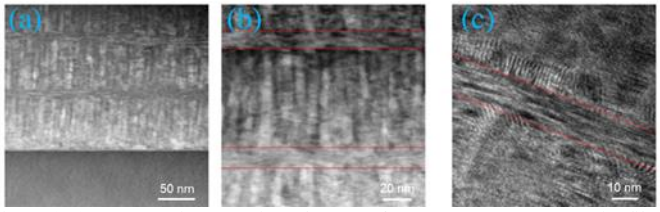


Fig. 3(a)–(c). TEM images of 6 vol.% BZO/YBCO ML nanocomposite film with the BZO doped layers of ~ 50 nm thickness, which were deposited with a laser repetition rate of 8 Hz; and the CaY123 spacer layers of ~ 10 nm thickness, which were deposited at a laser repetition rate of 2 Hz.

While the two CaY123 spacers truncate the BZO 1D–APCs in three segments through the ML film thickness, they have negligible effect on the alignment of the BZO 1D–APCs in different BZO/YBCO layers. This means the ML scheme, especially with the first BZO/YBCO layer grown in the exactly same way to that in BZO/YBCO SL nanocomposite film, would allow the formation of the BZO 1D–APCs in each of the three BZO/YBCO layers separated by the CaY123 spacers. In fact, the BZO 1D–APCs in the three BZO/YBCO layers have similar morphology, dimension, and orientation. Since the bottom BZO/YBCO layer was grown in the same way to that in the 6 % SL BZO/YBCO nanocomposite films, the BZO 1D–APCs in the ML and SL samples are expected to be similar in terms of concentration and dimension. The CaY123 spacers can also be seen in Fig. 3(a), and more zoom-in views in Fig. 3(b)–(c).

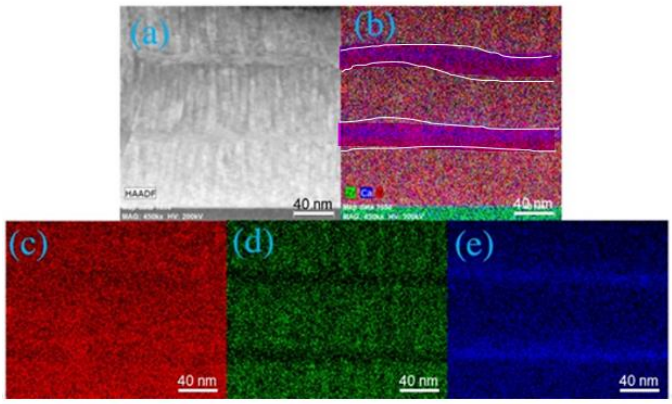


Fig. 4. Cross-sectional STEM image (a) and elemental maps (b)–(e) taken on a 6 vol. % BZO/YBCO ML nanocomposite film. (b) is the combined element map of Y (red), Zr (green), and Ca (blue) while (c–e) exhibit the separate maps of the three elements. The multilayer film consists of ~ 50 nm thick BZO layers deposited with a repetition rate of 8 Hz and ~ 10 nm CaY123 layers deposited with a laser repetition rate of 2 Hz.

Fig. 4(a)–(e) display the morphology and element distribution of a 6 % BZO/YBCO ML film in the cross-sectional view. Fig. 4(a) shows that the BZO 1D–APCs formed through the thickness of each of the three BZO/YBCO layers even with the truncation by the CaY123 spacers. This is further supported by the Zr distribution shown in Fig. 4(b) and 4(d), which means the concentration of the BZO 1D–APCs in the ML sample would be comparable to that of their SL counterpart at the same BZO doping. Fig. 4(e) shows most Ca remains in the CaY123 spacers while a minute amount may diffuse into the BZO/YBCO layers.

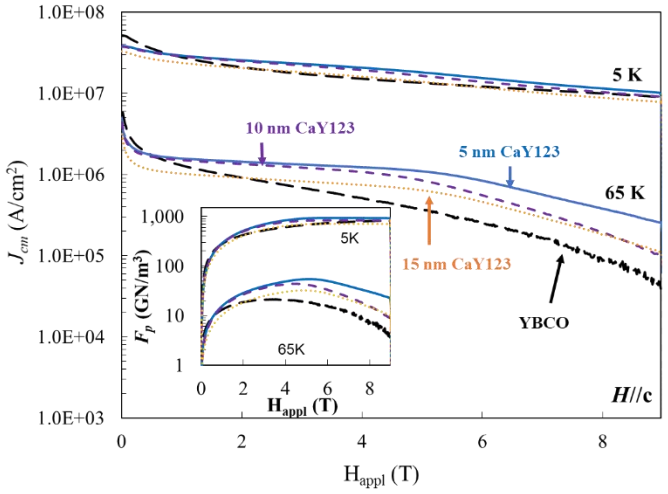


Fig. 5 Comparison of magnetically measured $J_c$(H) and $F_p$(H) on reference YBCO (black) and 6 vol. % BZO/YBCO ML (colored) films of varying spacer layers of 5 nm, 10 nm, and 15 nm at H//c-axis.

Fig. 5 compares the $J_c$(H) curves measured at 5 K and 65 K on the three 6 % ML samples shown in Fig. 2(a) with CaY123 spacer thickness varied from 5 nm (blue solid), 10 nm (purple small dash) and 15 nm (orange dot). For comparison, the $J_c$(H) curve measured on a reference YBCO film (black large dash) is also included in Fig. 5. While the four samples show more or less comparable $J_c$(H) at 5 K, the ML samples exhibit

© 2023 IEEE. Personal use is permitted, but republication/redistribution requires IEEE permission. See https://www.ieee.org/publications/rights/index.html for more information.
Authorized licensed use limited to: University of Kansas Libraries. Downloaded on March 25,2023 at 14:26:22 UTC from IEEE Xplore. Restrictions apply.

This article has been accepted for publication in IEEE Transactions on Applied Superconductivity. This is the author's version which has not been fully edited and content may change prior to final publication. Citation information: DOI 10.1109/TASC.2023.3258369



significantly enhanced $J_c$(H) at 65 K, especially at high H fields. For example, at 9 T, the ML sample with 5 nm of CaY layer (shown in blue line) has $J_c$ value of 0.22 MA/cm$^2$ which is about 7 times enhancement of the value of 0.032 MA/cm$^2$ in the reference YBCO sample.

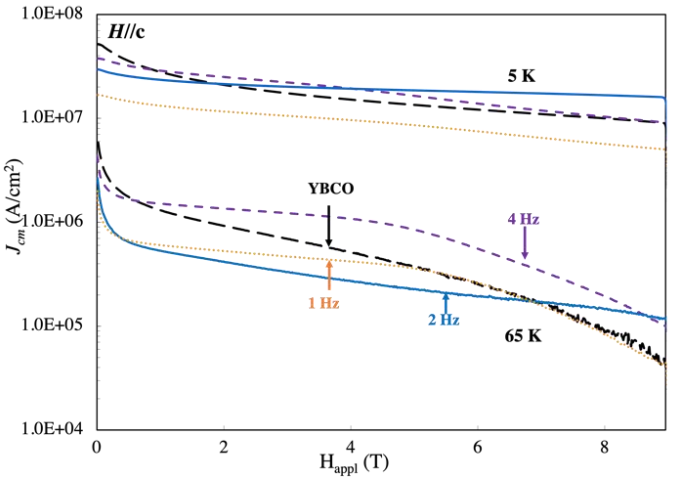


Fig. 6. Comparison of $J_c$(H) for reference YBCO (black long dash) and 6 vol.% BZO/YBCO ML films (colored) of varying repetition rates of 1 Hz, 2 Hz, and 4 Hz with 10 nm of CaY123 spacer layer thickness at the different magnetic field (H).

Fig. 6 compares the $J_c$(H) curves measured at 5 K and 65 K on the three 6 % ML samples shown in Fig. 2(b) with 10 nm CaY123 spacer thickness while varied PLD repetition rates of 1 Hz (orange dot), 2 Hz (blue solid) and 4 Hz (purple small dash). The $J_c$(H) curve measured on a reference YBCO film (black long dash) is also included in Fig. 6 for comparison. Remarkably, the ML samples show enhanced $J_c$(H) at both temperatures of 5 K and 65 K. For example, at 65 K and at 9 T, a $J_c$ enhancement of 2.2 times for the ML sample (0.11 MA/cm$^2$) is obtained as compared to the YBCO reference sample (0.039 MA/cm$^2$). At 5 K, this enhancement is higher at ~2.9 times with $J_c$~16.06 MA/cm$^2$) for the ML sample as compared with the $J_c$~7.45 MA/cm$^2$ for the reference YBCO sample. This result is important since it reveals that the improvement of APC/YBCO interface for improved pinning efficiency [17], [27] leads to enhanced $J_c$(H) not only at temperatures near $T_c$, but also at lower temperatures up to 5 K.

Fig. 7 compares the $J_c$(H) measured on the reference YBCO (black long dash), 6 % BZO/YBCO SL (blue solid) and ML (purple small dash) samples. At 65 K, both BZO SL and ML samples show much-enhanced $J_c$ values when the field is greater than 2 T. In comparison with the SL sample, the ML sample has further enhanced $J_c$ over the entire field range, which suggests the ML approach is beneficial to further improving pinning efficiency of the BZO 1D–APCs. Interestingly, the 6 % BZO/YBCO SL sample exhibits a slightly lower $J_c$(H) than that of the reference YBCO at 5 K, which indicates growth defects in the reference YBCO may provide equivalent or better pinning to the BZO 1D–APCs in the 6 % BZO/YBCO SL sample. This result indicates the importance to understand the correlation between crystal structure and pinning properties as revealed in a recent systematic study [28]. Remarkably, the 6 % BZO/YBCO ML sample shows higher $J_c$(H) than the other two samples at 5 K in almost the entire H range. Interesting, at self-field and low fields up to ~0.3 T, the reference YBCO has a higher $J_c$ than both BZO/YBCO samples, suggesting further investigation of crystal structures of BZO/YBCO samples is important for a fully controlled pinning landscape.

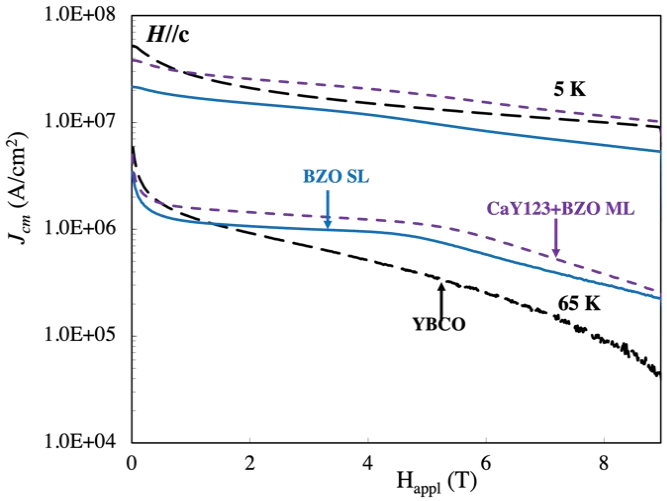


Fig. 7. $J_c$ (H) comparison of YBCO film (black long dash), 6 vol.% BZO/YBCO SL film (blue solid), and 6 vol.% BZO/YBCO ML film (purple short dash) at 5 K and 65 K respectively. All measurements were carried out at H//c-axis. All samples have a comparable thickness of 150–170 nm. For the ML sample, the CaY123 spacer layer thickness is 5 nm made at 4 Hz PLD repetition rate.

## CONCLUSIONS

In summary, this work investigates the pinning properties of the 6 vol.% BZO/YBCO ML nanocomposite films in comparison with their 6 vol.% BZO/YBCO SL counterpart's and reference YBCO samples at 5 K and 65 K. The ML films fabricated at various CaY123 layer thicknesses of 5–15 nm and at different laser repetition rates of 1, 2, and 4 Hz were included to understand the effect of those parameters on the pinning properties of the ML films. Overall enhanced $J_c$ (H) have been observed on all ML samples as compared to their SL BZO/YBCO nanocomposite counterparts and the reference YBCO film at both 5 K and 65 K over most range of the applied magnetic field up to 9 T. This result suggests the ML approach is promising to improve the APC/YBCO interface for better pinning.

## REFERENCES

[1] X. Obradors and T. Puig, "Coated conductors for power applications: materials challenges," *Supercond. Sci. Technol.*, vol. 27, no. 4, Mar. 2014, Art. no. 044003.

[2] D. Uglietti, "A review of commercial high temperature superconducting materials for large magnets: from wires and tapes to cables and conductors," *Supercond. Sci. Technol.*, vol. 32, no. 5, 2019, Art. no. 053001.

[3] J. L MacManus-Driscoll and S.C. Wimbush, "Processing and application of high-temperature superconducting

© 2023 IEEE. Personal use is permitted, but republication/redistribution requires IEEE permission. See https://www.ieee.org/publications/rights/index.html for more information.
Authorized licensed use limited to: University of Kansas Libraries. Downloaded on March 25,2023 at 14:26:22 UTC from IEEE Xplore. Restrictions apply.

This article has been accepted for publication in IEEE Transactions on Applied Superconductivity. This is the author's version which has not been fully edited and content may change prior to final publication. Citation information: DOI 10.1109/TASC.2023.3258369



coated conductors," *Nat. Rev. Mater.*, vol. 6, no. 7, Mar. 2021, p. 587-604.

[4] P. Mele, et al., "Ultra-high flux pinning properties of $BaMO_3$-doped $YBa_2Cu_3O_{7-x}$ thin films (M= Zr, Sn)," *Supercond. Sci. Technol.*, vol. 21, no. 3, Feb. 2008, Art. no. 032002.

[5] J. MacManus-Driscoll, et al., "Strongly enhanced current densities in superconducting coated conductors of $YBa_2Cu_3O_{7-x}$+ $BaZrO_3$," *Nat. Mater.*, vol. 3, no. 7, May 2004, p. 439-443.

[6] J. Wu, and J. Shi, "Interactive modeling-synthesis-characterization approach towards controllable in situ self-assembly of artificial pinning centers in RE-123 films," *Supercond. Sci. Technol*., vol. 30, no. 10, Sep. 2017, Art. no. 103002.

[7] S. Miura, et al., "Strongly enhanced irreversibility field and flux pinning force density in $SmBa_2Cu_3O_y$-coated conductors with well-aligned $BaHfO_3$ nanorods," *Appl. Phys. Express*, vol. 10, no. 10, Sep. 2017, Art. no. 103101.

[8] S. Chen, et al., "Generating mixed morphology $BaZrO_3$ artificial pinning centers for strong and isotropic pinning in $BaZrO_3$–$Y_2O_3$ double-doped YBCO thin films," *Supercond. Sci. Technol*., vol. 30, no. 12, Nov. 2017, Art. no. 125011.

[9] B. Gautam, et al., "Transformational dynamics of BZO and BHO nanorods imposed by $Y_2O_3$ nanoparticles for improved isotropic pinning in $YBa_2Cu_3O_{7-\delta}$ thin films," *AIP Adv.*, vol. 7, no. 7, 2017, Art. no. 075308.

[10] B. Gautam, et al., "Probing the effect of interface on vortex pinning efficiency of one-dimensional $BaZrO_3$ and $BaHfO_3$ artificial pinning centers in $YBa_2Cu_3O_{7-x}$ thin films," *Appl. Phys. Lett*., vol. 113, no. 21, Nov. 2018, Art. no. 212602.

[11] S. Chen, et al., "Enhancement of isotropic pinning force in YBCO films with $BaZrO_3$ nanorods and $Y_2O_3$ nanoparticles," *IEEE T. Appl. Supercon*., vol. 27, no. 4, Nov. 2016, Art. no. 8000205.

[12] E. Galstyan, et al., "Pinning Characteristics of Zr and Hf-Added REBCO Coated Conductors Made by Advanced MOCVD in Low-to-High Magnetic Fields," *IEEE Trans. Appl. Supercon.*, vol. 31, no. 5, Aug. 2021, Art. no. 8000405.

[13] M. A. P. Sebastian, et al., "Study of the Flux Pinning Landscape of YBCO Thin Films With Single and Mixed Phase Additions $BaMO_3$+ Z: M= Hf, Sn, Zr and Z= $Y_2O_3$, Y211," *IEEE Trans. Appl. Supercon.*, vol. 27, no. 4, Jun. 2017, Art. no. 7500805.

[14] C. Cantoni, et al., "Strain-driven oxygen deficiency in self-assembled, nanostructured, composite oxide films," *ACS nano*, vol. 5, no. 6, May 2011, p. 4783-4789.

[15] A. K. Jha and K. Matsumoto, "Interfaces in REBCO-Based Nanocomposite Thin Films and their Contribution to Vortex Pinning," *Surfaces and Interfaces of Metal Oxide Thin Films, Multilayers, Nanoparticles and Nano-composites*, Sep. 2021, Springer, p. 205-221.

[16] J. Wu, J., B. Gautam, and V. Ogunjimi, "Pinning Efficiency of Artificial Pinning Centers in Super-conductor Nanocomposite Films, *Superconductivity: From Materials Science to Practical Applications,*" P. Mele, et al., Editors, 2020, Springer International Publishing: Cham. p. 29-52.

[17] V. Ogunjimi, et al., "Enhancing magnetic pinning by $BaZrO_3$ nanorods forming coherent interface by strain-directed Ca-doping in $YBa_2Cu_3O_{7-x}$ nanocomposite films," *Supercond. Sci. Technol.*, vol. 34, no. 10, Sep. 2021, Art. no. 104002.

[18] M. Panth, et al., "Multilayer $YBa_2Cu_3O_{7-x}$/$Ca_{0.3}Y_{0.7}$ $Ba_2Cu_3O_{7-x}$ Nanocomposite Films With 2–8% $BaZrO_3$ Doping for High-Field Applications," *IEEE T. Appl. Supercon.*, vol. 32, no. 8, Nov. 2022, Art. no. 8001208.

[19] J. Z. Wu, et al., "Enabling coherent $BaZrO_3$ nanorods/$YBa_2Cu_3O_{7-x}$ interface through dynamic lattice enlargement in vertical epitaxy of $BaZrO_3$/$YBa_2Cu_3O_{7-x}$ nanocomposites," *Supercond. Sci. Technol*., vol. 35, no. 3, Feb. 2022, Art. no. 034001.

[20] V. Ogunjimi, et al., "Enhancing magnetic pinning by $BaZrO_3$ nanorods forming coherent interface by strain-directed Ca-doping in $YBa_2Cu_3O_{7-x}$ nanocomposite films," *Supercond. Sci. Technol*., vol. 34, no. 10, Sep. 2021, Art. no. 104002.

[21] M. Panth, et al. "Temperature dependent pinning efficiency in multilayer and single layer BZO/YBCO nanocomposite films," *IOP Conf. Ser. - Mater. Sci.,* vol. 1241, no. 1, May 2022, Art. no. 012021.

[22] X. Wang, et al., "Eliminating thickness dependence of critical current density in $YBa_2Cu_3O_{7-x}$ films with aligned $BaZrO_3$ nanorods," *J. Appl. Phys*., vol. 108, no. 11, Dec. 2010, Art. no. 113911.

[23] J. Kell, T. Haugan, M. Locke, P. Barnes, "Tb and Ce doped Y123 films processed by pulsed laser deposition," *IEEE Trans. on Appl. Supercond.,* vol. 15, no. 2, Jun. 2005, pp.3726-3729.

[24] C. Bean, "Magnetization of hard superconductors," *Phys. Rev. Lett*., vol. 8, no. 6, Mar. 1962, pp. 250-253.

[25] C. Bean, "Magnetization of high field superconductors," *Rev. Mod. Phys*., vol. 36, Jan. 1964, pp. 31-39.

[26] A. K. Jha, et al., "Tailoring the vortex pinning strength of YBCO thin films by systematic incorporation of hybrid artificial pinning centers," *Supercond. Sci. Technol.*, vol. 28, no. 11, Oct. 2015, Art. no. 114004.

[27] J. Z. Wu, et al., "Enabling coherent $BaZrO_3$ nanorods/$YBa_2Cu_3O_{7-x}$ interface through dynamic lattice enlargement in vertical epitaxy of $BaZrO_3$/$YBa_2Cu_3O_{7-x}$ nanocomposites," *Supercond. Sci.Technol*., vol. 35, no. 3, Feb. 2022, Art. no. 034001.

[28] P. Paturi and H. Huhtinen, "Roles of electron mean free path and flux pinning in optimizing the critical current in YBCO superconductors," *Supercond. Sci. Technol*., vol. 35, no. 6, 2022, Art. no. 065007.

© 2023 IEEE. Personal use is permitted, but republication/redistribution requires IEEE permission. See https://www.ieee.org/publications/rights/index.html for more information.
Authorized licensed use limited to: University of Kansas Libraries. Downloaded on March 25,2023 at 14:26:22 UTC from IEEE Xplore. Restrictions apply.